The Interaction of Formic Acid with Zinc Oxide: A Combined Experimental and Theoretical Study on Single Crystal and Powder Samples

8 AUTHORS, INCLUDING:

Heshmat Noei
Deutsches Elektronen-Synchrotron
35 PUBLICATIONS **478** CITATIONS

Alexei Nefedov
Karlsruhe Institute of Technology
107 PUBLICATIONS **1,105** CITATIONS

Yuemin Wang
Ruhr-Universität Bochum
99 PUBLICATIONS **2,423** CITATIONS

Christof Wöll
Karlsruhe Institute of Technology
551 PUBLICATIONS **17,492** CITATIONS

ORIGINAL PAPER

The Interaction of Formic Acid with Zinc Oxide: A Combined Experimental and Theoretical Study on Single Crystal and Powder Samples

**Maria Buchholz · Qiang Li · Heshmat Noei ·
Alexei Nefedov · Yuemin Wang · Martin Muhler ·
Karin Fink · Christof Wöll**

Abstract We present azimuth- and polarization-dependent infrared spectroscopy results obtained under ultra-high vacuum conditions on surface species formed by the interaction of formic acid with the mixed-terminated $ZnO(10\bar{1}0)$ surface. Since there are no previous IRRAS data for formic-acid derived species on any ZnO single crystal surfaces, we have carried out calculations using density function theory to aid the interpretation of the results. From our combined experimental and theoretical data we conclude that two different formate species are formed. The more strongly bound species is a bidentate with the formate molecular plane oriented along the $[1\bar{2}10]$ direction. The less strongly bound species is a quasi-bidentate with its molecular plane oriented along the [0001] direction. This second species is characterized by a strong hydrogen bond between a surface OH species and the formate. In addition, IR data were recorded for the same molecule adsorbed on commercial ZnO nanoparticles. The different bands of the powder IR-data are assigned on the basis of the experimental and theoretical results obtained for the single crystal surface. This study demonstrates the importance of the Surface Science approach to heterogeneous catalysis also for ZnO, an important catalyst for the conversion of syngas to methanol.

Keywords Zinc oxide · Infrared · IRRAS · DFT · Formic acid

M. Buchholz · A. Nefedov · C. Wöll (✉)
Institute of Functional Interfaces, Karlsruhe Institute of Technology, 76021 Karlsruhe, Germany
e-mail: christof.woell@kit.edu

Q. Li · K. Fink
Institute of Nanotechnology, Karlsruhe Institute of Technology, 76021 Karlsruhe, Germany

H. Noei · Y. Wang · M. Muhler
Laboratory of Industrial Chemistry, Ruhr-University Bochum, 44780 Bochum, Germany

H. Noei
Deutsches Elektronen-Synchrotron (DESY), 22607 Hamburg, Germany

Y. Wang
Department of Physical Chemistry I, Ruhr-University Bochum, 44780 Bochum, Germany

1 Introduction

A detailed understanding of the adsorption properties of molecules on ZnO surfaces is of fundamental interest in the field of heterogeneous catalysis as well as for the optimization of dye-sensitized solar cells (DSSCs). The interaction of formic acid (HCOOH) with ZnO surfaces can be considered a model case relevant for both of these fields. On the one hand, in one of the technologically most important catalytic conversion processes, methanol is produced via a catalytic reaction over a $Cu/ZnO/Al_2O_3$-catalyst from synthesis gas $(CO/CO_2/H_2)$. Here, surface-bound HCOO* and HCOOH* are proposed to be important intermediate species [1, 2]. Note that although today the industrially relevant catalytic process is carried out using Cu/ZnO catalysts, also ZnO without copper catalyzes the conversion of syngas to methanol [3]. On the other hand, formic acid on ZnO serves as a good model system to study the grafting of carboxylic acids to oxidic substrates. One of the prominent examples for the importance of acid/oxide interactions are DSSCs (Grätzel-cell) [4–6]. The dye

molecules used in these cells are anchored via a carboxyl group to the substrate. Gaining more detailed knowledge about the anchoring of the dye to the substrate is of crucial importance for improving the stability of ZnO-based DSSCs. Although the interaction of formic acid with ZnO has been addressed by several groups, experimental studies of the system are rather scarce [7–10].

In previous works a number of different possible formate structures have been proposed to result from the dissociative adsorption of formic acid on ZnO($10\bar{1}0$) surfaces. Structural models of the proposed structures are shown in Fig. 1, which is furthermore used to define the terminology used throughout the article.

The bidentate formate (structure I), where the oxygen atoms of the acid are bound to the Zn atoms along the [$1\bar{2}10$]-direction, is the structure which has been proposed in most of the previous theoretical studies on metal oxides [11, 12] and in particular on ZnO [13–15]. The quasi-bidentate formate along the [0001]-axis (Fig. 1, structure II), occasionally also referred to as unidentate, has been favored in the theoretical studies by Persson et al. [14, 15]. Here, the formate is bound via the carbonyl oxygen to a zinc atom of the surface and via the hydrogen of the hydroxyl group to oxygen of the substrate.

The monodentate, where the formate is bound via the oxygen to a zinc atom of the surface, could exist as cis- or trans-isomer (Fig. 1, structure III) [8, 10]. In the Hartree–Fock (HF) calculations of Nakatsuji et al. this structure was found to be unstable [13]. The formate could also exist as a

chelate, where both oxygen atoms of the acid are bound to one Zn atom (Fig. 1, structure IV). (Here we use the chemical description of a chelate which is different from the description of Crook et al., where this configuration is referred to a bidentate [8]). The chelate could be oriented along the [$1\bar{2}10$]- or the [0001]-direction. Another possible bidentate could be bound over an oxygen vacancy along the [0001]-direction. This geometry was found as one of the stable configurations for formic acid on anatase-TiO$_2$ (101) [16].

On the basis of near-edge-X-ray-absorption fine structure (NEXAFS) spectroscopy, it has been proposed that HCOOH deprotonates yielding a formate species with a nearly upright standing geometry on the ZnO($10\bar{1}0$) surface [7]. On the basis of this data, Davis et al. proposed the presence of a chelate species with its molecular plane oriented along the [0001] direction. In another experimental study Crook et al. investigated the formic acid adsorption on the ZnO($10\bar{1}0$)-surface at room temperature with high resolution electron energy loss spectroscopy (HREELS). They observed vibrations at 1040, 1363, 1573 and 2895 cm^{-1}, which were assigned to π(CH), ν_s(OCO), ν_{as}(OCO) and ν(CH)-modes, respectively [8]. Similar results were obtained with perdeuterated formic acid (DCOOD), namely vibrations at 1330, 1580 and 2154 cm^{-1}, which were assigned to ν_s(OCO), ν_{as}(OCO) and ν(CD)-modes of DCOO species, respectively [8]. Previous infrared spectroscopy measurements of the adsorption of formic acid on ZnO powder particles showed rather broad bands assigned to the
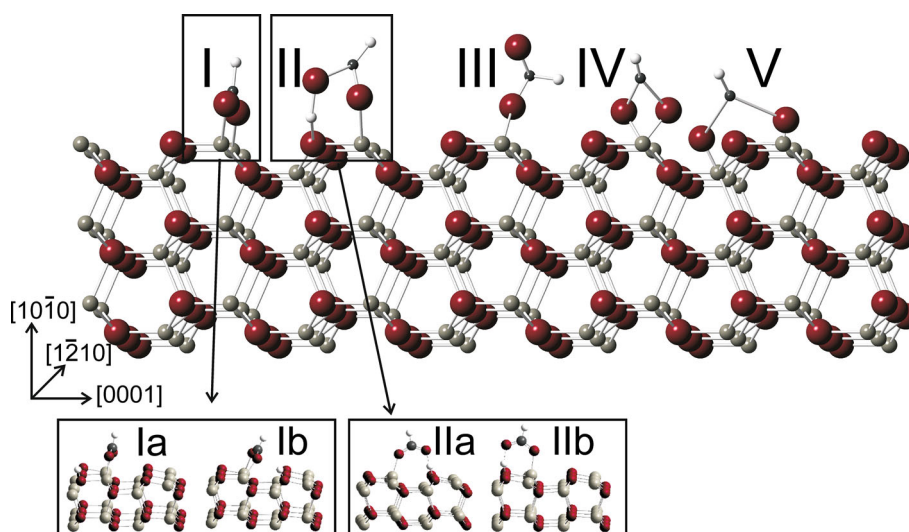

Fig. 1 Ball-stick model of potential adsorption configurations of dissociated formic acid on ZnO($10\bar{1}0$). Structure I is a bidentate, structure II a quasi-bidentate, structure III a monodentate, structure IV a chelate, and structure V a bridge bidentate. The bidentate and the quasi-bidentate are investigated more in detail in dependence on the position of the proton (bidentate a (Ia), bidentate b (Ib), quasi-bidentate a (IIa) and quasi-bidentate b (IIb)). The quasi-bidentate is a formate, which is bound via the carbonyl oxygen to a zinc atom of the surface and via the hydrogen of the hydroxyl group to oxygen of the substrate. Color code: red oxygen, grey zinc, black carbon and white hydrogen

asymmetric carboxylate stretching vibration at 1589 cm^{-1} and the symmetric at 1350 cm^{-1}. From comparison with vibrational frequencies calculated with density functional theory (DFT/B3LYP) for a $Zn_{10}O_{10}$ cluster they assigned a bidentate species [9]. However, for this hybrid functional the size of cluster which can be treated is rather limited.

Embedded cluster calculations using a wave-function based approach in connection with Møller–Plesset second order perturbation theory (MP2) were performed on a Zn_4O_4 cluster by Nakatsuji et al. and revealed a bidentate as well as a quasi-bidentate formate species [13] with almost identical binding energies (E_{BE}) of 79 kcal/mol. In their calculations the chelate formate configuration was found to be unstable. For the free formic acid molecule two conformations exist: *cis*-formic acid, where both protons are on the same side, and *trans*-formic acid where the protons are on opposite sides. Whereas for the free molecule the *cis*-form is the most stable conformation, for adsorbed formic acid the trans-confirmation was found to be favored, because the proton is closer to the oxygen atom of the substrate and can form a hydrogen bond [13]. Periodic Hartree–Fock calculations reported by Persson et al. revealed that a tilted bidentate formate is more stable than the quasi-bidentate [14]. Later Persson et al. also investigated a chelate formate configuration which was in comparison to the other structures only weakly bound to the surface (30 kcal/mol) [15]. To summarize, all calculations reported so far revealed dissociative adsorption forming formate species with a strong bond between adsorbate and surface.

In order to identify which of the previous models mainly proposed on theoretical grounds is correct and in order to be able to interpret the—rather complex—IR spectra reported for ZnO powders, an application of the Surface Science approach is needed [17]. This approach requires high-quality reference data for well-defined single crystal surfaces. Although data from HREELS have been reported, the application of this technique suffers from the rather intense Fuchs–Kliewer phonons modes [18]. Moreover, the somewhat limited resolution of HREELS makes the interpretation of IR data recorded for powders difficult. For this reason we have carried out a study using infrared reflection absorption spectroscopy (IRRAS). In recent works the huge potential of polarization- and azimuth-dependent IRRAS data was demonstrated for carbonate species of CO_2 on ZnO(10$\bar{1}$0) [19] and for formic acid adsorbed on r-TiO$_2$(110) [12]. The interpretation of IRRAS data is straight-forward, in the case of metal substrates as only vibrations with a transition dipole moment (TDM) perpendicular to the surface can be detected (so called metal surface selection rule) [20, 21]. In contrast to metal surfaces, the situation on oxides (or dielectrics) is much more complicated. For a detailed analysis the interaction of three different components of the incident light

with the TDM of a particular vibration has to be considered. The s-polarized component of the incident light is oriented parallel to the surface and perpendicular to the incidence direction. Only vibrations with a non-zero component of the TDM oriented perpendicular to the incidence plane can be observed with s-polarized light. For p-polarized light the situation is more complex. The p-polarized component of the incident light consists of a tangential component $p_{t,x}$ and a normal component $p_{n,z}$. Only vibrations with a component of their TDM oriented perpendicular to the surface can interact with the $p_{n,z}$-component [19]. Depending on the azimuthal orientation, vibrations with TDM parallel to the surface can be excited either by $p_{t,x}$- or by s-polarized light.

In order to aid the assignment of the experimentally observed features we have additionally performed DFT calculations on adsorption energies and frequencies. It is investigated which is the most stable adsorption geometry of formic acid on zinc oxide, in particular on ZnO(10$\bar{1}$0). The mixed-terminated (10$\bar{1}$0) ZnO surface was chosen for the experimental and theoretical studies, because it is the thermodynamically most stable surfaces [22]. In addition, since the largest fraction of the surfaces exposed by ZnO powder particles exhibits this (10$\bar{1}$0) orientation, the data for this mixed-terminated surface are particularly useful for interpretation of ZnO powder IR spectra. In the present paper we describe the use of polarized IR light incident along both high-symmetry azimuths of the ZnO(10$\bar{1}$0) surface in order to provide detailed information about the adsorption geometry of formic acid on the surface.

2 Experimental

For our experiments we used two different infrared measurement geometries. On the single crystal, IR-spectra were recorded in reflection geometry, while transmission geometry was used in the case of ZnO powder particles.

2.1 UHV-IRRAS Experiments for ZnO(10$\bar{1}$0)

The IRRAS studies on the ZnO(10$\bar{1}$0) single crystal were performed using an UHV-system (Prevac, Rógow, Poland) equipped with a state-of-the-art IR spectrometer (Bruker Vertex 80v, Bruker Optics, Ettlingen, Germany). The IR-spectrometer is directly coupled to the UHV-chamber (base pressure of 1×10^{-10} mbar) via differentially pumped KBr-windows. Samples can be cooled down to 50 K with liquid helium or to 100 K with liquid nitrogen. Photo-electron spectroscopy studies (X-ray photoelectron spectroscopy (XPS), Ultraviolet photoelectron spectroscopy (UPS), Auger electron spectroscopy (AES)) can be performed in the analysis chamber (R4000 analyzer,

VGScienta, Uppsala, Sweden) of the same UHV-system. One of the two preparation chambers is equipped with a LEED/AES-System Model 800 (OCI Vacuum Microengineering, London, Canada).

The ZnO(10$\bar{1}$0)-single crystal (Mateck, Jülich, Germany) was prepared as described in detail in Ref. [19]. The cleanliness of the substrate was checked by XPS (Zn 2p$_{3/2}$ = 1021.8 eV and O1 s = 530.7 eV (SI, Fig. 1)). The structural quality was checked with LEED (1 × 1 pattern) (see SI, Fig. 2). Formic acid (99.9 %, Merck, Darmstadt, Germany) was additionally cleaned via pump-freeze-thaw-cycles and dosed via backfilling of the IR-chamber through a leak valve.

For the IRRAS data, 2048 scans were accumulated in grazing incidence (80°) geometry with a resolution of 4 cm^{-1}. All spectra were taken at room temperature. All IRRAS data shown in the present paper correspond to difference spectra which were obtained by subtracting a background recorded immediately before exposure to formic acid.

2.2 UHV-FTIR Experiments for Powders

The IR spectra of formic acid adsorbed on ZnO powder particles were recorded using another, but similar UHV-Fourier Transform Infrared spectroscopy (FTIRS) system (Prevac, Rógow, Poland, base pressure 2 × 10^{-10} mbar) [23]. The ZnO powder samples (ZnO NanoTek ®) were first pressed into a gold-plated stainless steel grid and then mounted on a sample holder specially designed for the FTIR transmission measurements under UHV conditions. Prior to each exposure, a spectrum of the bare ZnO particles was used as a background reference. All UHV-FTIR spectra were collected with 1024 scans at a resolution of 2 cm^{-1} in transmission mode.

2.3 Computational Method

All DFT calculations were performed with the Vienna ab initio Simulation Package (VASP) [24–26]. The generalized gradient approximation with the functional described by Perdew and Wang [27] (GGA-PW91) was used for all calculations. The projector-augmented wave (PAW) method [28] is applied to describe the wavefunctions in the core regions, while the valence wavefunctions are expanded as linear combination of plane-waves with a cutoff energy of 400 eV. In the geometry optimizations of the wurtzite cell of ZnO, the total energy was converged to 10^{-5} eV and the Hellmann–Feynman force on each relaxed atom was less than 1 meVÅ^{-1}. The equilibrium lattice constants (a = 3.285 Å, c = 5.297 Å and the internal parameter u = 0.3793) are similar to PBE results (a = 3.282 Å, c = 5.291 Å, u = 0.3792) [29] and agree well with the experimental values (a = 3.2496 Å, c = 5.2042 Å and u = 0.3819) [30].

Based on the optimized bulk cell and lattice constants, the surface calculations were performed using a slab model, consisting of 8 layers of Zn–O, followed by a vacuum layer with a width of 10 Å. The positions of all atoms besides the oxygen atoms of the deepest layer (see Fig. 3 in SI) were optimized, until the Hellmann–Feynman forces converged to 0.01 eV Å^{-1}. During optimization surface Zn atoms of the uppermost layer move downwards; the distance between Zn and O atoms of the surface layer is 0.35 Å and agrees well with experimental data (0.4 Å) [31]. To prevent lateral interactions between formic acid molecules on the surface, a supercell with a size of 3 × 2 (96 atoms) was used in the calculations. The Brillouin zone was sampled with a (3 × 3 × 1) Monkhorst–Pack [32] mesh of k-points for the supercell calculations. With help of density-functional perturbation theory (DFPT) or linear response (LR) theory [33, 34], vibrational spectra can be determined, as well as the tensor of the Born effective charges [35], which is used to obtain the intensities of the vibrations [36]. Because frequency calculations are very time-consuming, only the first layer of Zn–O was involved. In selected cases test calculations were carried out where a second layer of ZnO was considered. In all cases the differences in the calculated frequencies were below 2 cm^{-1}.

The E$_{BE}$ of the adsorbate to the surfaces were calculated by using

$$E_{BE} = E_{(HCOOH/ZnO)} - (E_{HCOOH} + E_{ZnO}).$$

Here, E$_{(HCOOH/ZnO)}$ denotes the total energy of the respective HCOOH/ZnO adsorbate configuration, E$_{ZnO}$ is the total energy of the clean ZnO surface, and E$_{HCOOH}$ is the total energy of the HCOOH molecule with trans-configuration, which was obtained in a 10 Å × 10 Å × 10 Å sized cell using Γ-point approximation.

3 Results and Discussion

3.1 UHV-IRRAS Results on ZnO(10$\bar{1}$0)

The azimuth- and polarization dependent IRRA spectra of 5 L formic acid exposed to ZnO(10$\bar{1}$0) at 300 K are shown in Fig. 2. For IR light incident along the [1$\bar{2}$10] direction, a positive signal at 1573 cm^{-1} and a negative signal at 1374 cm^{-1} can be observed with p-polarized light. Only one negative signal at 1577 cm^{-1} is observed with s-polarized light. The observed vibrations are characteristic for the formate species and are assigned to the asymmetric and symmetric carboxylate stretch vibrations, respectively [8]. The IR data reveal that formic acid adsorbs dissociatively on ZnO(10$\bar{1}$0) yielding formate species.
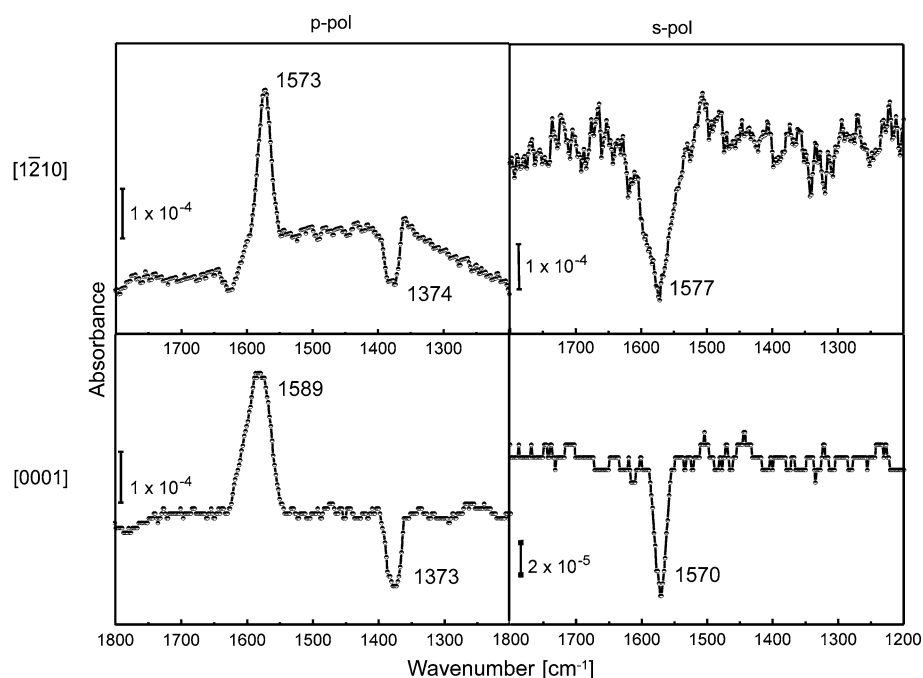
For the IR beam incident along the [0001]-axis, the spectra are very similar and also show two signals for p-polarized light (Fig. 2): one positive at 1589 cm^{-1} and one negative at 1373 cm^{-1}. In the spectrum with s-polarized light, only one negative signal can be seen at 1570 cm^{-1}. Since no vibration between 1600 and 1800 cm^{-1} originating from the ν(C=O) mode is observed; a monodentate configuration can be already excluded.

The two vibrational bands at 1589 and 1373 cm^{-1} indicate the presence of a bidentate formate species, because of a typical wavenumber splitting around 200 cm^{-1}. In the following, we will demonstrate that the experimental IR-data cannot be explained by the presence of just one bidentate formate species (as in the case of carbonate species formed by interaction of the same single crystal substrate with CO$_2$ [19]). To this end we show in Fig. 3 the signals expected for the bidentate species I (see Fig. 1) using the reflectivity calculations described in Ref. [19]. The solid line indicates the signals expected for an orientation of the formate molecular plane strictly perpendicular to the surface, the dotted line shows the situation for a tilted (45°) species. In case of a substantial tilt angle the major difference is that the symmetric stretch vibration can also be excited with s-polarized light along the [$1\bar{2}10$] azimuth, whereas the asymmetric stretch vibration still can only be seen with s-polarized light along the [0001] direction or with p-polarized light along the [$1\bar{2}10$] direction.

In particular from the presence of only one strong peak for p-polarized light along the [0001]-azimuth we can conclude that the formation of formate species on
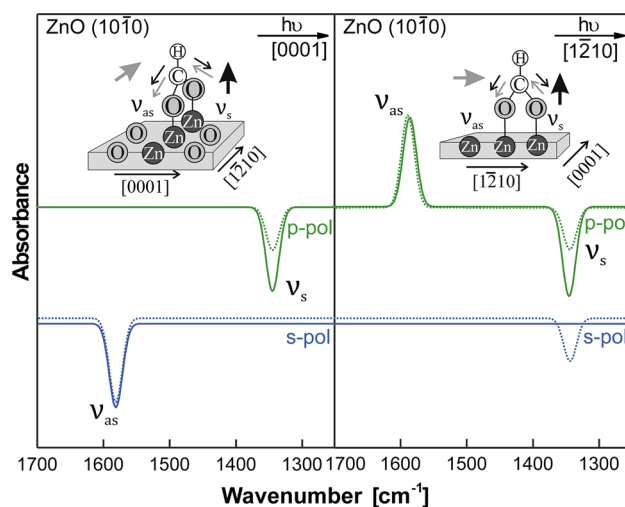

Fig. 3 Expected signals in IRRA spectra based on reflectivity calculations [19] for the bidentate configuration oriented along the [$1\bar{2}10$] direction. The expected vibrational carboxylate signals for an incidence beam along the [0001] azimuth (*left panel*) and along the [$1\bar{2}10$] azimuth are shown (*right panel*). The *dotted lines* show the expected spectral features for a bidentate with its molecular axis tilted by 45°. The adsorption configuration is sketched with *arrows* indicating the vibration movements. The transition dipole moments are indicated by a *big light* and *dark grey arrow* for the asymmetric, respectively the symmetric carboxylate stretching vibration

ZnO($10\bar{1}0$) cannot be described by only one adsorption geometry, even if a substantial tilt of the bidentate is present (see above). Later we will discuss this point more in detail.

3.2 UHV-FTIRS Results for ZnO Powders

Figure 4 shows the UHV-FTIRS data obtained after HCOOH adsorption on the clean NanoTek-ZnO powder at 300 K. NanoTek-ZnO has a rod shape hexagonal structure dominated by the non-polar mixed-terminated ZnO(10$\bar{1}$0) surface [37]. The formation of formate species is clearly identified by the typical IR bands at 1624, 1580, 1380 and 1365 cm^{-1} [7, 8]. Their assignments will be discussed in the Sect. 4 based on the experimental and theoretical results for ZnO single crystals. Additionally, the ν(C–H) vibration was observed at 2873 cm^{-1}. Because of the low intensity of this band, it could not be observed in the IRRA spectra obtained with the ZnO single crystal. The presence of formate species is further supported by the heating experiments (Fig. S4 in SI). The corresponding IR bands disappear only upon heating to 600 K, which is in line with the thermal stability of formate on ZnO reported in the literature [38].

3.3 DFT Calculations

In order to gain further inside into adsorption geometries and the corresponding IR spectra, DFT calculations were performed starting from the structures reported in literature [9, 13–15]. Several possible configurations were considered and minimum energy structures located. The optimized structures and their relative energies ΔE with respect to the lowest minimum are given in Tables 1 and 2, respectively. The lowest energy was found for the bidentate conformation Ia (left hand side of Fig. 1) where dissociated formic acid is adsorbed along the [1$\bar{2}$10]- direction of the ZnO(10$\bar{1}$0) surface. The bidentate b differs by the position of the hydrogen transferred to the surface. The interaction of the surface hydrogen with the formate influences the
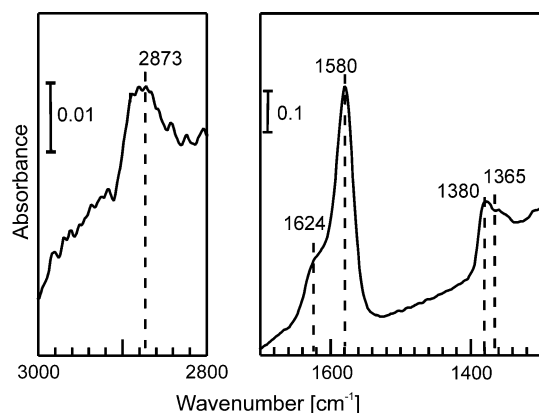

Fig. 4 UHV-FTIR spectra obtained after exposing the clean ZnO nanoparticles to 5×10^{-5} mbar HCOOH at 300 K in an UHV chamber

adsorption energy by up to 0.2 eV. These changes in ΔE are of the same order as for bidentate configurations on the (110) surface of rutile-TiO$_2$ where changes of around 0.3 eV [12] were observed. The bidentates are tilted to the surface, the tilt angles are 23° and 25° in respect to the surface normal for bidentate a, respectively bidentate b. These values agree much better with NEXAFS results (23°) [7] than periodic HF calculations (15°) [14]. The second stable configurations regarding the energy are the quasi-bidentates IIa and IIb. They stand upright without any tilt to the surface.

In the case of the quasi-bidentate formate configuration along the [0001] direction (Fig. 1, structure II), the dissociated hydrogen is transferred from the formic acid to a surface oxygen in such a way that it still can form a hydrogen bond to one oxygen of the formate while the other formate oxygen binds directly to a surface Zn atom. The former can either bind to the Zn and the OH group of a surface ZnO dimer with a distance of 2.00 Å (ΔE = 7.97 kcal/mol) or form a bridge between two surface dimers. In the latter case, the Zn–O distances of the Zn adsorption site and the OH group amounts to 3.43 Å and it is with ΔE = 11.13 kcal/mol less stable. In Table 2 the E$_{BE}$ with respect to the energy of a formic acid molecule and the ZnO(10$\bar{1}$0) surface of the different bidentate and quasi-bidentate conformations are compared with the HF calculations of Persson et al. [14] and Nakatsuji et al. [13]. Both, the bidentate and the quasi-bidentate adsorption geometries are stable with respect to desorption. The HF cluster calculations of Nakatsuji show significantly stronger E$_{BE}$, while our results are on the same order as the values obtained by Persson. For the two quasi-bidentates the opposite energetic order was observed. The origin might be the neglect of dynamic correlation in the HF calculations. Additionally, a chelate configuration (Fig. 1, structure IV) with both oxygen atoms connected to one Zn atom was investigated. It oriented along the [1$\bar{2}$10] direction during the structure optimization. It has a relative energy of ΔE = 14.97 kcal/mol compared to the bidentate a. However, a negative force constant was observed in the frequency calculations indicating a saddle point. Structure V (see Fig. 1) is a bidentate formate bridging two Zn–O surface dimers. In this structure the oxygen atom of the dissociated formic acid cannot approach the sub-layer Zn close enough to form a stable bond because of the repulsive interaction from the surface oxygen atoms. In order to reduce this repulsion, the Zn atom moves out on top of the surface. Structure V was found to be ΔE = 35.14 kcal/mol higher in energy than structure I.

For all four structures (bidentate and quasi-bidentate) the vibrational frequencies and their intensities have been calculated. The results are shown in Fig. 5. The lines represent the peak positions of the vibrational frequencies

Table 1 Optimized minimum structures and relative energies (kcal/mol) with respect to bidentate a
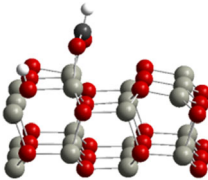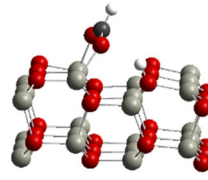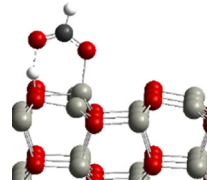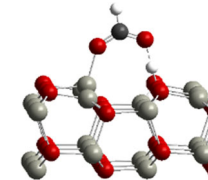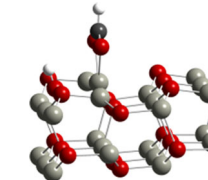
Bidentate a (Ia)	Bidentate b (Ib)	Quasi-bidentate a (IIa)	Quasi-bidentate b (IIb)	Chelate (IV)
ΔE = 0.00	ΔE = 4.54	ΔE = 7.97	ΔE = 11.13	ΔE = 14.97

Table 2 Binding energies with different configurations and methods

Structure	Adsorption Energy (kcal/mol)		
	Nakatsuji et al. (a)	Persson et al.(b)	This work
Bidentate a (Ia)	−79.8	−52.4 (−45.5)(c)	−42.91
Bidentate b (Ib)			−38.37
Quasi-bidentate a (IIa)	−79.6	−40.7	−34.94
Quasi-bidentate b (IIb)		−46.1	−31.78

in the range from 1300 to 1700 cm^{-1}. The height of the lines refers to the intensities. The assignment of the vibrations is indicated for all peaks and observed by analysis of the normal coordinates. Furthermore, the frequency splitting of the symmetric and asymmetric carboxylate stretching vibrations $\Delta(\nu_{as}-\nu_s)$ are given. For structures Ia, Ib, and IIa the carboxylate frequencies are rather similar and the splitting amounts to 250 cm^{-1}. Only for structure IIb $\Delta(\nu_{as}-\nu_s) = 198$ cm^{-1} is significantly smaller.

4 Discussion

In our study we considered five different adsorption geometries (Fig. 1) which have been discussed for the adsorption of formic acid on oxidic surfaces in literature.

Since the experimental IR spectra in Figs. 2 and 4 do not show a ν(C=O) stretching vibration between 1600 and 1800 cm^{-1} we exclude the monodentate (structure III). In our calculations the chelate structure IV was found to correspond to a saddle point with an imaginary vibrational frequency. It is therefore not a stable geometry and can be excluded from further discussion. For structure V the binding energy is much lower than for structure I. Accordingly, we feel that we can rather safely also exclude this structure from the further discussion.

In the quantum chemical calculations a bidentate formate (structure I) adsorbed along the [1$\bar{2}$10] direction and a quasi-bidentate formate (structure II) along the [0001] were found

to be most stable (see Table 1). Based on the experimental results and theoretical calculations, it is concluded that the vibration signals around 1570 cm^{-1} are assigned to the asymmetric carboxylate stretching vibration, the signals around 1370 cm^{-1} to the symmetric stretching vibration of formate species, revealing the dissociative adsorption of HCOOH on ZnO(10$\bar{1}$0) at 300 K [8, 11, 12, 16].

In the following we thus will consider only structures I and II. As already discussed above, the presence of structure I is consistent with the experimental data but there must be at least one more species present. Below we will show that the presence of structure I and structure II together can explain the experimental data. The sign of the vibrational signals can be explained by the reflectivity calculations of Ref. [19]. Note that the component of the TDM perpendicular to the surface can only couple to the $p_{n,z}$ component of the incident light and results in a negative signal. The component of the TDM parallel to the surface can couple either to the $p_{t,x}$ or the s-polarized light, depending on the direction of this component and the direction of the incident light.

For a bidentate formate as depicted in Fig. 1 the ν_{as}(OCO) vibration should for an incident beam along [0001] be visible with s-polarized light and the ν_s(OCO) vibration with $p_{n,z}$-polarized light. The positive band seen for the ν_{as}(OCO) with p-polarized light cannot be due to this species, even if a tilt of the bidentate is considered (see the simulations shown in Fig. 3).

We will therefore now additionally consider the second most stable structure found in the calculations. For the quasi-bidentate the TDM of the ν_{as}(OCO) is oriented along the [0001]-direction (Fig. 6) and can therefore couple to the $p_{t,x}$-component for light incident along the [0001]-azimuth leading to a positive band. As illustrated in Fig. 3, also for the other azimuth the presence of the two species is fully consistent with the signs of the asymmetric and symmetric stretch bands seen in the experimental data.

Of course, in principle one would expect the frequencies of the ν_s(OCO) and ν_{as}(OCO) vibrations of these two

Fig. 5 Simulated IR spectra of four optimized minimum structures
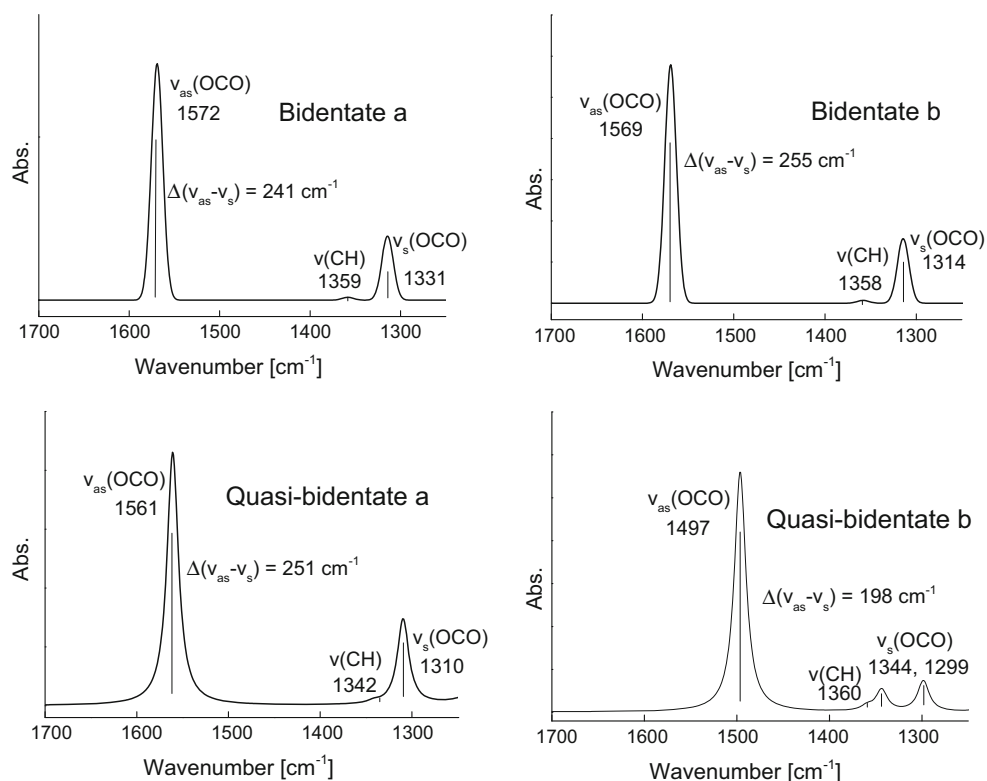
different formate species to be slightly different. Table 3 shows the assignment of the carboxylate stretch vibrations. In the DFT calculations, however, the carboxylate frequencies of the bidentate and the quasi-bidentate structures were found to be rather similar (see Fig. 5). The wavenumber splitting of the calculated signal amounts to $\Delta = 241$ cm^{-1} for the most stable configuration of the bidentate and $\Delta = 251$ cm^{-1} for the quasi-bidentate, respectively. This is slightly higher than the experimental values of $\Delta = 199$ cm^{-1} [1$\bar{2}$10] (197 cm^{-1} [0001]) for the bidentate and $\Delta = 203$ cm^{-1} [1$\bar{2}$10] (216 cm^{-1} [0001]) for the quasi-bidentate. However, the value of the splitting is still characteristic for a bidentate formate [39, 40]. The calculations as well as the experimental data show a larger wavenumber splitting for the quasi-bidentate than for the bidentate, which could be explained by the additional interaction with the proton which is bound to the surface.

The calculations prove that the positions of the hydrogen on the surface have a great influence on the splitting. The effect is more pronounced for $\nu_s(OCO)$ compared to $\nu_{as}(OCO)$. For example, the difference of $\nu_{as}(OCO)$ for bidentate (a) and (b) is negligible, however, for $\nu_s(OCO)$ it is 17 cm^{-1}. To investigate the influence of the H position on the IR spectra, we positioned the hydrogen as far away from the formate as it was possible within the chosen supercell and obtained 1571 and 1333 cm^{-1} for $\nu_{as}(OCO)$ and $\nu_s(OCO)$, respectively. The differences are within 2 cm^{-1} compared to
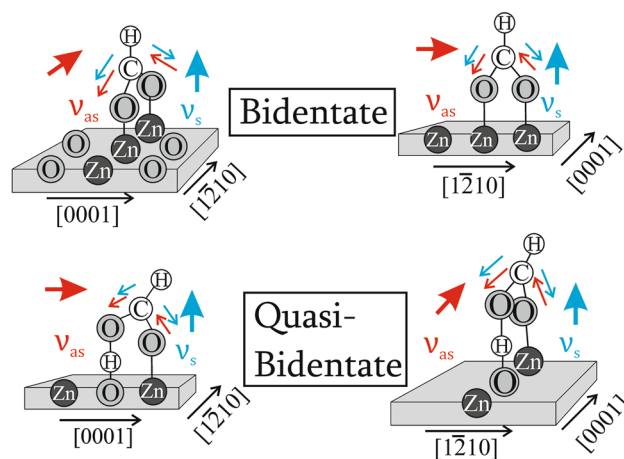

Fig. 6 Sketch of the possible adsorption geometries, the quasi-bidentate and the bidentate. *Red small arrows* show the direction of the asymmetric stretching vibration, the *big red arrow* indicates the orientation of transition dipole moment (TDM). *Blue small arrows* show the direction of the symmetric stretching vibration, the *blue arrow* indicates the orientation of TDM

bidentate *a*, however, a blueshift of 19 cm^{-1} is observed for bidentate *b*, which has a enhanced interaction between the surface OH species and the formate.

Finally, the vibration signals in the powder IR spectra were assigned with the help of the single-crystal spectra and the DFT-calculations (Fig. 7). The most intense IR bands at 1580 cm^{-1} (which shifts to 1571 cm^{-1} at 350 K

Table 3 Assignment of the experimental carboxylate vibrations in dependence of the incident radiation, the polarization and the orientation of the adsorption configuration

	$\nu_{as}(OCO)$ [cm^{-1}]		$\nu_s(OCO)$ [cm^{-1}]	
	$p_{t,x}$	s	$p_{n,z}$	
Bidentate along [1$\bar{2}$10]	1573	1570	1374	Beam along [1$\bar{2}$10]
			1373	Beam along [0001]
Quasi-Bidentate along [0001]	1589	1577	1374	Beam along [1$\bar{2}$10]
			1373	Beam along [0001]

Fig. 7 Comparison of the obtained infrared single-crystal data of formic acid on ZnO(10$\bar{1}$0) with infrared powder data, for the incident beam along [0001] (*left*) and along [1$\bar{2}$10] (*right*). The intensity of IR-single crystal data is multiplied by a factor of 2,000 to compare it with the powder IR data

(see SI, Fig. 4)) and at 1365 cm^{-1} could be attributed to the formation of (quasi-) bidentate formate species via the dissociative adsorption of HCOOH on the most prominent surface of the nanoparticles, namely the (10$\bar{1}$0)-surface. In addition, a weak band was observed at 1624 cm^{-1}, which is characteristic for a monodentate formate and is assigned to the ν(C=O) mode. The monodentate formate species could be formed on the polar terminated ZnO surfaces [8, 41, 42]. Here the formate is bound via one oxygen atom to a Zn^{2+} surface cation (Lewis acid). The IR band at 1380 cm^{-1} is assigned to the C–H bending mode δ(C–H) of HCOO, which is not sensitive to the types of formate species on oxide surfaces [16, 38], however it could not be observed in the single-crystal data. It should be noted that a proper assignment of the IR bands obtained for powder samples is challenging, since defects play an important role as active centers in these catalytically active powder particles. The formate species can also be formed via HCCOH dissociative adsorption on different defect sites such as steps, edges, kinks, and vacancies. However, the IR bands of these minor formate species could not be resolved in the present IR spectra (Fig. 4).

In addition, one dominant ν(C–H) stretching band is detected at 2873 cm^{-1}, which is also indicative of the formation of formate species. However, this mode is not sensitive to the surface structure and cannot provide detailed information about the different formate species.

5 Conclusions

From the comparison of the IR experimental data and DFT calculations we conclude that formic acid adsorbs dissociatively as formate on the mixed-terminated ZnO(10$\bar{1}$0) surface in two different orientations, which are perpendicular to each other. The bidentate structure which is oriented along the [1$\bar{2}$10] direction is most stable based on
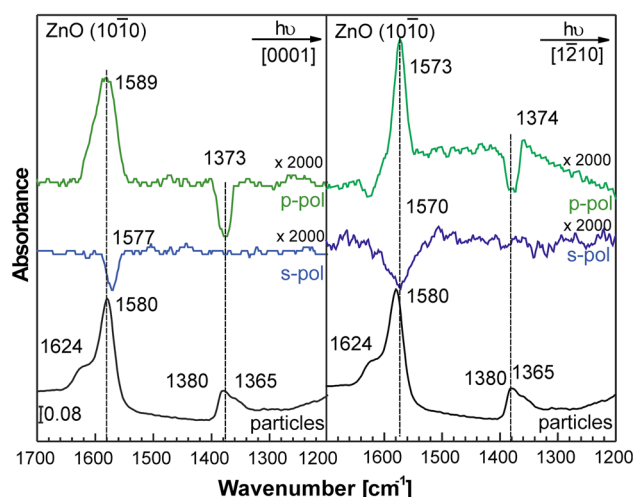
the DFT calculations. A quasi-bidentate, oriented along [0001], is found at slightly higher energies. Considering these two orthogonal orientations are in line with the experimental single crystal data. The azimuth- and polarization-dependent IR data, which can give detailed information about the adsorption geometry.

These results can be used to assign the bands observed in the complex powder IR spectra. For the latter it is not possible to differentiate between the quasi-bidentate and the bidentate because of the coexistence of different formate species on various facets and defects.

References

1. Hansen JB, Højlund Nielsen PE (2008) Methanol Synthesis. In: Handbook of Heterogeneous Catalysis. Wiley. doi:10.1002/9783527610044.hetcat0148
2. Grabow LC, Mavrikakis M (2011) Mechanism of methanol synthesis on Cu through CO$_2$ and CO hydrogenation. Acs Catal 1(4):365–384
3. Mittasch A, Pier M (1924) Synthetic manufacture of methanol. United States Patent US 1569775, 12. Jan 1926
4. Grätzel M (2001) Photoelectrochemical cells. Nature 414(6861):338–344
5. Grätzel M (2003) Dye-sensitized solar cells. J Photochem Photobio C 4(2):145–153
6. Anta JA, Guillén E, Tena-Zaera R (2012) ZnO-based dye sensitized solar cells. J Phys Chem C 116(21):11413–11425

7. Davis R, Walsh JF, Muryn CA, Thornton G, Dhanak VR, Prince KC (1993) The orientation of formate and carbonate on ZnO(10-10). Surf Sci 298(1):L196–L202

8. Crook S, Dhariwal H, Thornton G (1997) HREELS study of the interaction of formic acid with ZnO(10-10) and ZnO(000-1)-O. Surf Sci 382(1–3):19–25

9. Lenz A, Selegard L, Söderlind F, Larsson A, Holtz PO, Uvdal K, Ojamäe L, Kall PO (2009) ZnO nanoparticles functionalized with organic acids: an experimental and quantum-chemical study. J Phys Chem C 113(40):17332–17341

10. Teklemichael ST, McCluskey MD (2012) Compensation of acceptors in ZnO nanocrystals by adsorption of formic acid. J Phys Chem C 116(32):17248–17251

11. Hayden BE, King A, Newton MA (1999) Fourier transform reflection-absorption IR spectroscopy study of formate adsorption on TiO$_2$(110). J Phys Chem B 103(1):203–208

12. Mattsson A, Hu S, Hermansson K, Österlund L (2014) Adsorption of formic acid on rutile TiO2 (110) revisited: an infrared reflection-absorption spectroscopy and density functional theory study. J Chem Phys 140(3):034705

13. Nakatsuji H, Yoshimoto M, Umemura Y, Takagi S, Hada M (1996) Theoretical study of the chemisorption and surface reaction of HCOOH on a ZnO(10-10) surface. J Phys Chem 100(2):694–700

14. Persson P, Ojamae L (2000) Periodic Hartree–Fock study of the adsorption of formic acid on ZnO(10-10). Chem Phys Lett 321(3–4):302–308

15. Persson P, Lunell S, Ojamae L (2002) Quantum chemical prediction of the adsorption conformations and dynamics at HCOOH-covered ZnO(10-10) surfaces. Int J Quantum Chem 89(3):172–180

16. Xu MC, Noei H, Buchholz M, Muhler M, Wöll C, Wang YM (2012) Dissociation of formic acid on anatase TiO$_2$(101) probed by vibrational spectroscopy. Catal Today 182(1):12–15

17. Freund HJ, Kuhlenbeck H, Libuda J, Rupprechter G, Bäumer M, Hamann H (2001) Bridging the pressure and materials gaps between catalysis and surface science: clean and modified oxide surfaces. Top Catal 15(2–4):201–209

18. Wang Y, Kováčik R, Meyer B, Kotsis K, Stodt D, Staemmler V, Qiu H, Traeger F, Langenberg D, Muhler M, Wöll C (2007) CO$_2$ activation by ZnO through the formation of an unusual tridentate surface carbonate. Angew Chem Int Ed 46(29):5624–5627

19. Buchholz M, Weidler PG, Bebensee F, Nefedov A, Wöll C (2014) Carbon dioxide adsorption on a ZnO (10-10) substrate studied by infrared reflection absorption spectroscopy. Phys Chem Chem Phys 16:1672–1678

20. Greenler RG (1966) Infrared study of adsorbed molecules on metal surfaces by reflection techniques. J Chem Phys 44(1):310–315

21. Greenler RG, Snider DR, Witt D, Sorbello RS (1982) The metal-surface selection rule for infrared spectra of molecules adsorbed on small metal particles. Surf Sci 118(3):415–428

22. Wöll C (2007) The chemistry and physics of zinc oxide surfaces. Prog Surf Sci 82(2–3):55–120

23. Wang Y, Glenz A, Muhler M, Wöll C (2009) A new dual-purpose ultrahigh vacuum infrared spectroscopy apparatus optimized for grazing-incidence reflection as well as for transmission geometries. Rev Sci Instrum 80(11):113106–113108

24. Kresse G, Furthmüller J (1996) Efficient iterative schemes for ab initio total-energy calculations using a plane-wave basis set. Phys Rev B 54(16):11169–11186

25. Kresse G, Furthmüller J (1996) Efficiency of ab initio total energy calculations for metals and semiconductors using a plane-wave basis set. Comput Mater Sci 6(1):15–50

26. Kresse G, Hafner J (1993) Ab-Initio molecular-dynamics for open-shell transition-metals. Phys Rev B 48(17):13115–13118

27. Perdew JP, Wang Y (1992) Accurate and simple analytic representation of the electron-gas correlation-energy. Phys Rev B 45(23):13244–13249

28. Blöchl PE (1994) Projector augmented-wave method. Phys Rev B 50(24):17953–17979

29. Meyer B, Marx D (2003) Density-functional study of the structure and stability of ZnO surfaces. Phys Rev B 67(3):035403

30. Karzel H, Potzel W, Kofferlein M, Schiessl W, Steiner M, Hiller U, Kalvius GM, Mitchell DW, Das TP, Blaha P, Schwarz K, Pasternak MP (1996) Lattice dynamics and hyperfine interactions in ZnO and ZnSe at high external pressures. Phys Rev B 53(17):11425–11438

31. Duke CB, Meyer RJ, Paton A, Mark P (1978) Calculation of low-energy-electron-diffraction intensities from ZnO (1010).2. Influence of calculational procedure, model potential, and 2nd-layer structural distortions. Phys Rev B 18(8):4225–4240

32. Monkhorst HJ, Pack JD (1976) Special points for Brillouin-zone integrations. Phys Rev B 13(12):5188–5192

33. Baroni S, de Gironcoli S, Dal Corso A, Giannozzi P (2001) Phonons and related crystal properties from density-functional perturbation theory. Rev Mod Phys 73(2):515–562

34. Pick RM, Cohen MH, Martin RM (1970) Microscopic theory of force constants in adiabatic approximation. Phys Rev B 1(2):910–920

35. Gonze X, Lee C (1997) Dynamical matrices, born effective charges, dielectric permittivity tensors, and interatomic force constants from density-functional perturbation theory. Phys Rev B 55(16):10355–10368

36. Karhanek D, Bucko T, Hafner J (2010) A density-functional study of the adsorption of methane-thiol on the (111) surfaces of the Ni-group metals: II.Vibrational spectroscopy. J Phys Condens Matter 22(26):265006

37. Noei H (2010) Vibrational spectroscopic Studies on Adsorption and Reactions over ZnO—based Catalysts. Dissertation, Ruhr-Universität Bochum, Bochum

38. Kähler K, Holz MC, Rohe M, Strunk J, Muhler M (2010) Probing the reactivity of ZnO and Au/ZnO nanoparticles by methanol adsorption: a TPD and DRIFTS study. ChemPhysChem 11(12):2521–2529

39. Busca G, Lorenzelli V (1982) Infrared spectroscopic identification of species arising from reactive adsorption of carbon oxides on metal oxide surfaces. Mater Chem 7(1):89–126

40. Nakamoto K (2008) Applications in coordination chemistry. Infrared and Raman spectra of inorganic and coordination compounds. Wiley, Hoboken

41. Petrie WT, Vohs JM (1991) An HREELS investigation of the adsorption and reaction of formic acid on the (0001)-Zn surface of ZnO. Surf Sci 245(3):315–323

42. Koßmann J, Roßmüller G, Hättig C (2012) Prediction of vibrational frequencies of possible intermediates and side products of the methanol synthesis on ZnO(000$\bar{1}$) by ab initio calculations. The Journal of Chemical Physics 136 (3):034706